Journal of ELECTRONIC MATERIALS, Vol. 39, No. 9, 2010
DOI: 10.1007/s11664-010-1303-4
© 2010 TMS

# Synthesis and Electronic Properties of the Misfit Layer Compound $[(PbSe)_{1.00}]_1[MoSe_2]_1$

COLBY L. HEIDEMAN,[1] RAIMAR ROSTEK,[2] MICHAEL D. ANDERSON,[1,3] ANDREW A. HERZING,[3] IAN M. ANDERSON,[3] and DAVID C. JOHNSON[1,4]

1.—Department of Chemistry and Materials Science Institute, University of Oregon, Eugene, OR 97403, USA. 2.—Thermoelektrische Systeme, Fraunhofer Institut für Physikalische Messtechnik, Heidenhofstr. 8, 79110 Freiburg, Germany. 3.—Surface and Microanalysis Science Division, National Institute of Standards and Technology, 100 Bureau Drive, Gaithersburg, MD 20899, USA. 4.—e-mail: davej@uoregon.edu

An ultralow-thermal-conductivity compound with the ideal formula $[(PbSe)_{1.00}]_1[MoSe_2]_1$ has been successfully crystallized across a range of compositions. The lattice parameters varied from 1.246 nm to 1.275 nm, and the quality of the observed $00\ell$ diffraction patterns varied through the composition region where the structure crystallized. Measured resistivity values ranged over an order of magnitude, from 0.03 Ω m to 0.65 Ω m, and Seebeck coefficients ranged from $-181\ \mu V\ K^{-1}$ to $91\ \mu V\ K^{-1}$ in the samples after the initial annealing to form the basic structure. Annealing of samples under a controlled atmosphere of selenium resulted in low conductivities and large negative Seebeck coefficients, suggesting an $n$-doped semiconductor. Scanning transmission electron microscopy cross-sections confirmed the interleaving of bilayers of PbSe with Se-Mo-Se trilayers. High-angle annular dark-field images revealed an interesting volume defect, where PbSe grew through a region where a layer of $MoSe_2$ would be expected in the perfect structure. Further studies are required to correlate the density of these defects with the observed electrical properties.

**Key words:** Misfit-layered compounds, carrier properties, thermoelectrics, thin films

## INTRODUCTION

We were part of a team that recently reported exceptionally low thermal conductivity, between $0.06\ W\ m^{-1}\ K^{-1}$ and $0.18\ W\ m^{-1}\ K^{-1}$, in a family of misfit layer compounds $[(PbSe)_{1.00}]_m[MoSe_2]_n$. The only prior report of the thermal conductivity of a misfit layer compound indicated a significantly higher value, $0.8\ W\ m^{-1}\ K^{-1}$, for polycrystalline $[(Yb_{0.95}S_1)_{1.24}]_1[NbS_2]_1$. The difference between these values results from the low-temperature synthesis approach used to prepare the $[(PbSe)_{1.00}]_m$-$[MoSe_2]_n$ family of misfit layer compounds, which kinetically stabilizes a type of turbostratic disorder initially observed in $WSe_2$, where ultralow thermal conductivity was initially observed. Electrical properties have not previously been reported for any members of this family of compounds.

Misfit layer compounds containing interpenetrating structural units of MX and $TX_2$ are a potentially large family having the general formula $[(MX)_{1+y}]_m[TX_2]_n$, where M = Sn, Pb, Sb, Bi, and rare-earth metals; T = Ti, V, Cr, Nb, and Ta; and X = S and Se. The values of $m$ and $n$, respectively, represent the number of MX and $TX_2$ layers in the unit cell of the superstructure. Each $TX_2$ layer consists of a single (001)-oriented molecular layer of the transition-metal dichalcogenide, with the T cations in trigonal prismatic or octahedral

(Received July 20, 2009; accepted May 25, 2010; published online June 17, 2010)

interstices of nested close-packed layers of X anions, with AbA or AbC stacking sequences, respectively. (Here we use the convention that the stacking of the anion and cation sublattices are distinguished by representing the former in upper-case letters.) Each MX layer contains two distorted atomic planes of the rock-salt structure with (001) orientation. The rock-salt layers contain equal amounts of M and X atoms and are incommensurate with the close-packed X planes of the $TX_2$ chalcogen layers. The misfit parameter, $y$, represents the difference between the density of metal cations in their respective layers. Misfit parameters reported in the literature range from $y = 0.07$ to $y = 0.28$.[1,2] Prior reports of these compounds have focused on the unusual crystal structures resulting from the misfit between the two sublattices and the broad range of physical properties observed in misfit layer compounds.[3,4] High-temperature synthesis has been used to prepare these compounds, typically resulting in the formation of the $n = m = 1$ compound as an ordered three-dimensional solid. Many potential members of this class of compounds are metastable with respect to either the binary compounds, the $n = m = 1$ compound, or other ternary compositions. The $[(PbSe)_{1.00}]_m[MoSe_2]_n$ family of misfit layer compounds is metastable with respect to a mixture of binary compounds.

The metastability of these misfit layer compounds makes it challenging to obtain reproducible electrical properties, as annealing at high temperatures to achieve equilibrium is not possible. Optimization of thermoelectric properties in general is challenging due to the interdependence of the several properties influencing the final efficiency. Controlling carrier density, which affects every parameter contributing to $ZT$, the dimensionless figure of merit, is challenging for new materials because appropriate dopants need to be identified and the relationship among composition, dopant concentration, and carrier concentrations must be empirically determined. For bulk materials, the carrier transport properties can typically be controlled during synthesis. In thin films, however, such control is typically difficult to attain due to the limited reproducibility in the deposition process. One solution is to apply a postdeposition anneal where an excess of a bulk source of the same material is enclosed in a sealed ampoule with the thin film. The bulk source acts as a reservoir of volatile components during equilibration, so that the composition of the thin film approaches that of the bulk source.

Herein we report the ranges of phase formation and electrical properties measured for $[(PbSe)_{1.00}]_1[MoSe_2]_1$, the parent compound of the $[(PbSe)_{1.00}]_m[MoSe_2]_n$ family of misfit layer compounds, across its compositional range of stability. We also report the results of annealing experiments designed to reproducibly control the transport properties of $[(PbSe)_{1.00}]_1[MoSe_2]_1$.

## EXPERIMENTAL PROCEDURES

Thin films of $[(PbSe)_{1.00}]_1[MoSe_2]_1$ were prepared by alternately depositing elemental layers in an ultrahigh-vacuum chamber with background pressure during deposition of less than $10^{-4}$ Pa ($10^{-6}$ mbar). A Thermionic 3 kW electron beam gun was used to evaporate elemental lead and molybdenum at a rate of $\sim$0.04 nm s$^{-1}$ and $\sim$0.02 nm s$^{-1}$, respectively. A custom-built effusion cell was used to supply selenium vapor at a rate of $\sim$0.5 nm s$^{-1}$. The amount of each element deposited per layer was controlled by the length of time a shutter was kept open, and the deposition rates were monitored and controlled by a quartz crystal thickness monitor. A custom LabVIEW program running on a personal computer controlled the deposition process, sequentially opening and closing the shutters and rotating the substrate between sources to produce the repeating structure of Pb-Se-Mo-Se in each of the samples. This process was repeated until the desired sample thickness was obtained.

To deposit the quantity of each element to form the respective rock-salt-structured PbSe bilayer or $MoSe_2$ trilayer, the deposition system was calibrated for each constituent individually. For lead selenide, 80 alternating layers of selenium and lead were deposited in five different films where the thickness of each selenium layer was held constant, while the thickness of the lead layers was systematically increased by increasing the time the shutter was held open. The film composition was determined using a Cameca SX50 electron probe microanalyzer operated at 10 keV, 15 keV, and 20 keV, with a 20 nA beam current and 1 $\mu$m spot size.* The Stratagem data analysis program was used to extract the film composition from the variation of the relative characteristic x-ray intensities as a function of accelerating voltage.[5,6] Pure metals and compounds were employed as microanalysis standards. Ten independent measurements at different positions on the samples were averaged to determine the final composition. We interpolated between the experimental values to find the lead thickness required for a 1:1 ratio of Pb:Se. This process was then repeated for molybdenum and selenium, where the molybdenum thickness was varied while the selenium thickness was held constant, to determine the deposition parameters required to form a film with a 1:2 composition of Mo:Se. A linear relationship between the time that the shutters were kept open and the bilayer thicknesses that were determined using low-angle x-ray reflectometry enabled us to extrapolate to shutter times where one deposition

*Certain commercial equipment, instruments, or materials are identified herein. Such identification does not imply recommendation or endorsement by the National Institute of Standards and Technology, nor does it imply that the products are necessarily the best available for the purpose.

bilayer of elements was equal to one structural unit of each constituent.

The as-deposited samples were first annealed in a nitrogen dry-box to form the desired structure. The oxygen partial pressures during annealing were $<1\ \mu L\ L^{-1}$. The samples were then sealed in an evacuated quartz ampoule with a ~1000-fold excess of either $MoSe_2$ or PbSe powder, to provide a source of Se vapor. The ampoule was annealed at different temperatures and times. After each annealing step, room-temperature electrical properties of the thin-film samples were measured. Sheet resistivity measurements were performed using a standard van der Pauw method with a quartz substrate and a Greek cross pattern.[7,8] The Seebeck coefficient was determined on a neighboring rectangular pattern, where a temperature gradient was induced by cooling one end of the sample via the Peltier effect. Thermocouple junctions were used to measure both the resulting temperature gradient and the induced voltage. The Seebeck coefficient was calculated from the slopes of graphs of induced voltage measured across both the copper and the constantan leads versus the measured temperature difference.

Film structure and compound formation were probed with x-ray diffraction (XRD) using a Bruker D8 Discover diffractometer (Cu $K_\alpha$ radiation, wavelength $\lambda = 0.15418$ nm). A $\theta$-$2\theta$ configuration was used for high-angle x-ray diffraction, scanning in the range $10° \leq 2\theta \leq -65°$ with a step size of 0.05° and a counting time of 2 s per step. The incident beam was conditioned using 1 mm divergence and detector slits.

Cross-sectioned specimens for scanning (STEM) and conventional transmission electron microscopy (TEM) analysis were prepared using the small-angle cleavage technique,[9] followed by final cleaning and thinning using a FEI NOVA NanoLab 600 DualBeam™ FIB equipped with a Sidewinder ion column. Samples were thinned to approximately 300 nm using 30 kV accelerating voltage on the ion source, followed by a polishing step at 5 kV and final end pointing at 2 kV. Samples were plasma-cleaned using a Fischione model 1020 plasma cleaner for 5 min prior to analysis to remove any organic contamination.

The cross-sectioned specimens were characterized using STEM high-angle annular dark-field (HAADF) imaging in an FEI Titan 80-300™ TEM/STEM equipped with a double-hexapole, spherical aberration corrector (CEOS GmbH) operating at an accelerating voltage of 300 kV with a ~100 pm probe containing ~90 pA of current. To ensure proper orientation of the cross-sectioned film with respect to the electron probe, the specimen was tilted to the [011] zone axis of the single-crystal Si substrate.

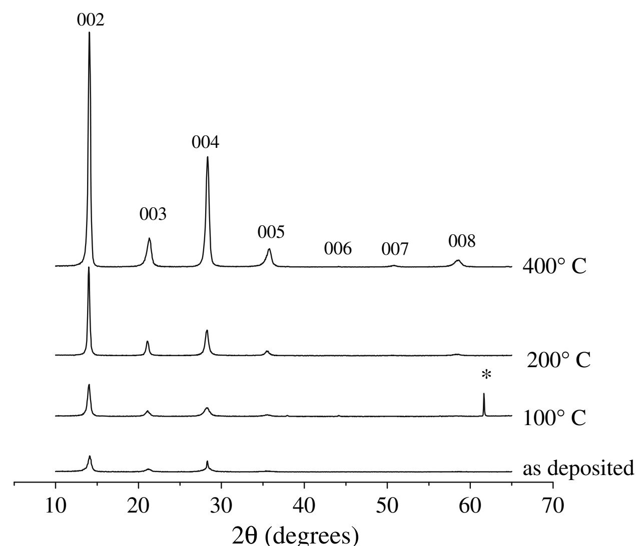


Fig. 1. Diffraction pattern for sample A as a function of annealing temperature. An identical intensity scale is used for each pattern, other than an offset to separate the patterns. Small crystallites are present upon deposition, which then grow as the sample is annealed at sequentially higher temperatures. The asterisk ("*") indicates the Si 400 $K_\beta$ reflection from the specimen substrate.

## RESULTS AND DISCUSSION

Once the deposition process was calibrated, many different $[(PbSe)_{1.00}]_1[MoSe_2]_1$ compounds were prepared, slightly varying the deposition process to determine the range of stoichiometries in which this compound could be synthesized. To determine the range of temperatures in which $[(PbSe)_{1.00}]_1$-$[MoSe_2]_1$ formed, a sample was annealed at a sequence of temperatures, and x-ray diffraction patterns were collected, as shown in Fig. 1. Initially, the film was primarily amorphous, with broad diffraction maxima indicating small crystallites nucleated during the deposition process. At temperatures below 200°C, little or no change occurred in the diffraction patterns. Between 200°C and 400°C, there was a significant increase in Bragg diffraction intensities, grain size, and crystallographic alignment with the *c*-axis of the misfit layer compound perpendicular to the substrate. Above 500°C in an open annealing system, crystallinity decreased as the samples began to decompose due to loss of selenium.

Using these data as a guide, all of the potential deposited samples were annealed and 21 of them clearly formed $[(PbSe)_{1.00}]_1[MoSe_2]_1$. The observed compositions all cluster around that calculated for $[(PbSe)_{1.00}]_1[MoSe_2]_1$, using the measured in-plane lattice constant of each component to calculate the density of atoms in the *a*-*b* plane of each constituent. Figure 2 shows the diffraction patterns for five of these films, exhibiting the range of peak widths and intensities obtained from the 21 samples. The lattice parameters ranged from 1.241 nm to 1.275 nm, as summarized in Table I, which also indicates the compositions, resistivities, and Seebeck coefficients for the compounds after annealing at 400°C in an oxygen-free dry-box.

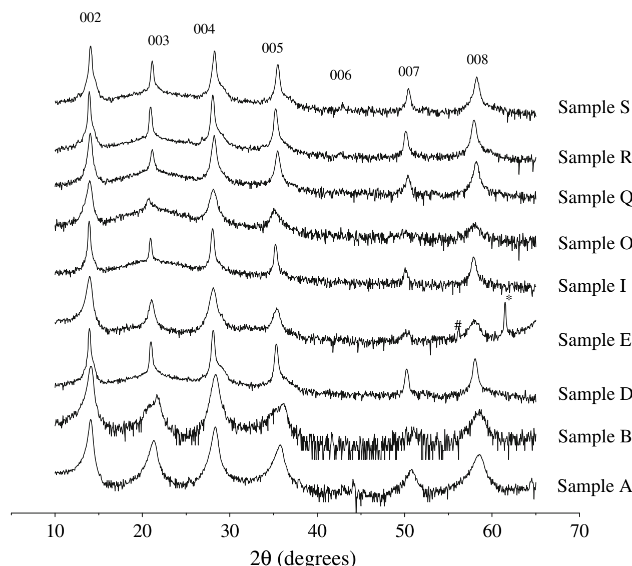


Fig. 2. Diffraction patterns obtained from nine different $[(PbSe)_{1.00}]_1[MoSe_2]_1$ samples. The vertical coordinate is the logarithm of the intensity, which enables the weaker Bragg peaks to be seen more easily. The symbols "#" and "⋆" indicate peaks resulting from the 400 Si substrate peak from W $L_\beta$ and Cu $K_\beta$ radiation, respectively, as confirmed on bare substrates. The W emission is believed to originate from contamination from the filament.

As can be seen from the data in Table I and the representative diffraction patterns, the single-phase field of the compound has a macroscopic range of homogeneity, with a corresponding range in lattice parameter, varying intensities between different $00\ell$-type Bragg diffraction peaks, and a significant spread in electrical properties from sample to sample. The resistivity values ranged over an order of magnitude, from 0.65 Ω m to 0.03 Ω m, and Seebeck coefficients ranged from $-181$ $\mu$V $K^{-1}$ to 91 $\mu$V $K^{-1}$ after the initial annealing to form the basic structure.

Given the variation in properties, we explored the effect of placing samples in a quartz ampoule under vacuum with a large excess of a bulk source of one of the components, effectively buffering the chemical activity. The samples were annealed with the goal of establishing equilibrium between the vapor pressure of the sample and that of the source. To determine the time required to reach equilibrium, three samples were annealed at 400°C for increasing amounts of time in the presence of lead selenide powder. Figure 3 shows the change in resistivity for these samples as a function of time. Equilibrium appears to be reached within 8 h. The data indicate that equilibrium is not diffusion limited at this annealing temperature, as sample thickness did not affect the rate of change of the properties, but that mass transfer through the vapor phase is the rate-limiting step. The difference in the final resistivities is a consequence of a corresponding difference in carrier concentrations, carrier mobilities, or a combination thereof.

To determine the effect of chemical activity on the electrical properties, sample D was annealed in a sealed quartz ampoule in the presence of a bulk

**Table I. $c$-Axis lattice parameters of 21 $[(PbSe)_{1.00}]_1[MoSe_2]_1$ samples, along with measured compositions, resistivity, and Seebeck coefficients, if measured**

| Sample | $c$-Lattice Parameter (nm) | Error | Resistivity (Ω m) | Seebeck Coefficient ($\mu$V $K^{-1}$) | Pb Content (at.%) | Mo Content (at.%) | Se Content (at.%) |
|---|---|---|---|---|---|---|---|
| A | 1.259 | 0.003 | | | 17 | 18 | 64 |
| B | 1.258 | 0.005 | | | 21 | 19 | 61 |
| C | 1.260 | 0.004 | | | | | |
| D | 1.2700 | 0.0003 | 0.20 | −181 | 20 | 20 | 60 |
| E | 1.269 | 0.002 | | | 20 | 20 | 60 |
| F | 1.269 | 0.001 | | | 21 | 19 | 60 |
| G | 1.268 | 0.002 | | | 20 | 20 | 59 |
| H | 1.275 | 0.003 | 0.20 | 91 | | | |
| I | 1.2730 | 0.0004 | 0.03 | | 22 | 24 | 54 |
| J | 1.275 | 0.005 | 0.18 | | | | |
| K | 1.273 | 0.007 | 0.20 | | 18 | 20 | 62 |
| L | 1.274 | 0.004 | 0.065 | | | | |
| M | 1.274 | 0.005 | 0.064 | | | | |
| N | 1.2731 | 0.0009 | 0.20 | | | | |
| O | 1.274 | 0.006 | 0.057 | | | | |
| P | 1.2727 | 0.0009 | 0.056 | | | | |
| Q | 1.265 | 0.002 | 0.051 | | | | |
| R | 1.2723 | 0.0004 | 0.062 | | | | |
| S | 1.265 | 0.002 | 0.061 | | | | |
| T | 1.246 | 0.001 | 0.65 | 35 | | | |
| U | 1.247 | 0.0001 | | | | | |

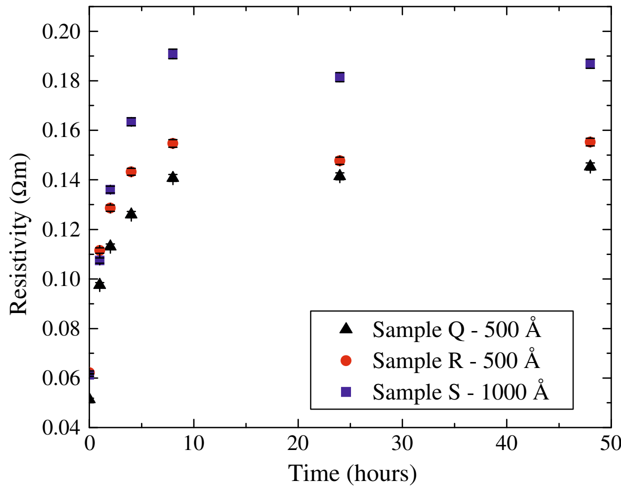


Fig. 3. Several $[(PbSe)_{1.00}]_1[MoSe_2]_1$ samples annealed in a sealed ampoule with PbSe powder serving as a selenium vapor source. Samples were sequentially annealed at increasing times until reaching equilibrium as indicated by the resistivity no longer changing.

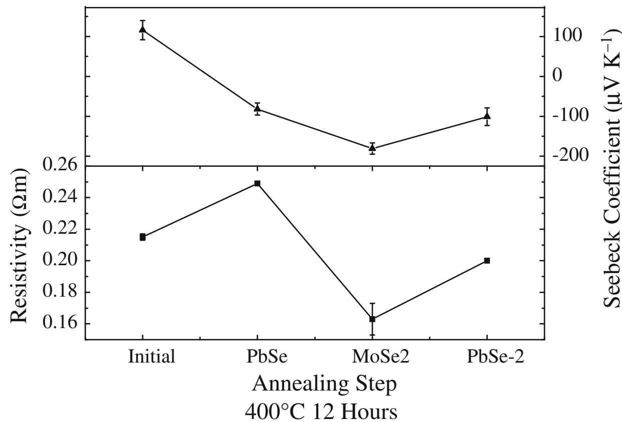


Fig. 4. Variation in resistivity and Seebeck coefficient during cyclic annealing of sample D in PbSe and $MoSe_2$ buffers. It was expected that the carrier concentration would vary with the chalcogen source. Initially, the sample had been annealed at 400°C for 30 min in a $N_2$ atmosphere to crystallize the film. Each subsequent annealing step was performed at 400°C for 12 h.

powder serving as a selenium vapor source, first with PbSe, then with $MoSe_2$, and finally again with PbSe. Each time the sample was annealed for 12 h at 400°C, long enough to achieve equilibrium. Transport properties were measured following each annealing step. We expected the selenium concentration within the film to vary with the different vapor sources due to differences in the vapor pressure of selenium from the different powders. This should lead to the carrier concentration changing slightly with the chalcogen vapor source.

Figure 4 shows the change in carrier properties resulting from the annealing sequence. During the annealing sequence, the Seebeck coefficient initially changes sign from 100 $\mu$V K$^{-1}$ to $-80$ $\mu$V K$^{-1}$ indicating that the majority carriers switch from holes to electrons. In the second annealing step, the magnitude of the Seebeck coefficient increases, indicating a decrease in the number of carriers when annealing with a $MoSe_2$ vapor source. In the final annealing step, the Seebeck coefficient returns to approximately 100 $\mu$V K$^{-1}$, indicating that the carrier concentration is set by the vapor source as expected.

The resistivity similarly tracks the annealing environment, increasing during the first annealing corresponding to a decrease in the total number of carriers. When annealing with $MoSe_2$ the resistivity decreases, and then increases again when annealing with PbSe, although not back to the original value observed after the first annealing step. In light of the Seebeck data, this likely results from an increase in the carrier mobility, leading to a lower resistivity for an equivalent number of carriers.

One challenge with the data interpretation presented to this point is that the Seebeck data indicate a larger carrier concentration when annealing with PbSe compared with $MoSe_2$ whereas the resistivity data indicates the opposite. It is possible that this discrepancy results from dopant segregation, which has been reported to lead to deviations in the Seebeck coefficient's dependence on the carrier concentration.[10] With the thin alternating layers present in these compounds, it would be unsurprising if dopants were not uniformly distributed through the structure.

While the electrical properties appear to vary with the annealing environment, the disparity in the properties between samples indicates the possible presence of structural defects that are not affected by the annealing process. To examine the local, atomic-scale structure of the films, STEM-HAADF images were acquired in an aberration-corrected electron microscope. As shown in Fig. 5, the cross-sectional STEM images are consistent with the x-ray diffraction evidence of a well-ordered structure along the *c*-axis, as the individual ~0.6-nm-thick structural units of the PbSe and $MoSe_2$ are clearly visible and oriented parallel to one another. In-plane rotational disorder is also apparent, as only on occasion are layers oriented at a low-index zone axis with respect to the incident beam, and different zone-axis orientations are observed within the field of view. The projected grain size, indicated by the spatial extent in the *a*-*b* plane of the individual orientations within a particular layer, is on the order of 10 nm to 100 nm. While Fig. 5 is consistent with a well-ordered misfit layer compound in the *c*-direction, the STEM-HAADF images also indicate interesting local defects. Regions are apparent where the rock-salt-structured layer appears to grow through the $MoSe_2$ layer. However, because the two components are of comparable size, the long-range stacking is not disturbed. This type of defect may result in broadening of the $00\ell$ diffraction peaks, as the coherence length of the structure is reduced by the difference

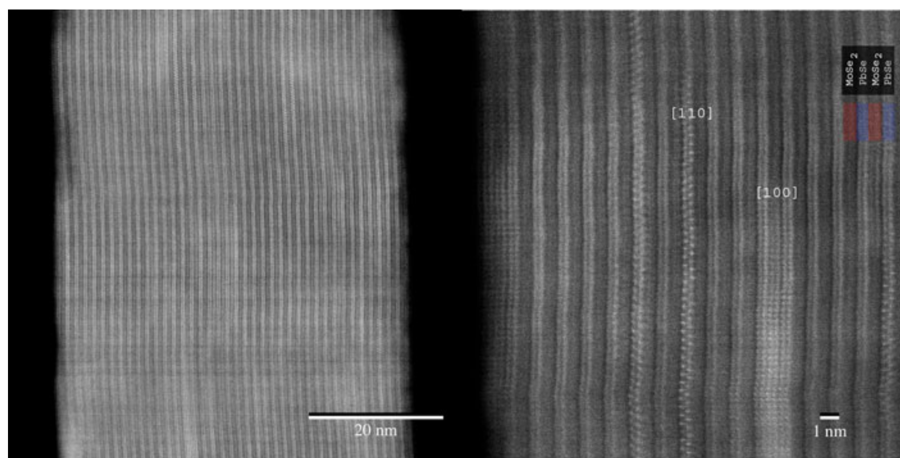


Fig. 5. STEM-HAADF images collected on $[(PbSe)_{1.00}]_1[MoSe_2]_1$ sample U. The alternating ~0.6 nm layers of the PbSe and $MoSe_2$ constituents are clearly visible. In the right-hand image, different in-plane orientations of the constituent structural units are apparent, as different zone axes of the PbSe layers are visible in different layers. Most layers are not orientated along a low-index zone axis. An interruption in the stacking sequence (*right*), where a PbSe layer partially occupies a region where a $MoSe_2$ layer would be expected in the perfect structure, is clearly apparent.

in the thickness of the constituent layers. Our current hypothesis is that differences in the concentration of this type of defect may be responsible for the broad range of electrical properties observed in this study, but further investigation is required to correlate the density of these defects with electrical properties.

## CONCLUSIONS

XRD data show that the misfit layer compound with the ideal formula $[(PbSe)_{1.00}]_1[MoSe_2]_1$ forms over a range of composition, leading to a spread of lattice parameters and to differences in the quality of the $00\ell$ diffraction patterns. Electrical properties vary considerably, presumably due to differences in defect concentrations caused by the spread in composition. Annealing under a controlled atmosphere of selenium produced samples with low conductivities and large negative Seebeck coefficients, suggesting an $n$-doped semiconductor. The spread of composition, lattice parameters, and electrical properties suggest the presence of volume defects in the films. STEM-HAADF images confirm the layered structure with alternating layers of PbSe and $MoSe_2$ in $[(PbSe)_{1.00}]_1[MoSe_2]_1$, consistent with the XRD studies. STEM images also show occasional interruption in the stacking sequence, where PbSe partially occupies a region where $MoSe_2$ would be expected in the perfect structure. Further studies will be required to correlate the concentration of these defects with the observed electrical properties.

## ACKNOWLEDGEMENTS

The Office of Naval Research (N0014-07-1-0358) supported this work. Colby Heideman and Michael Anderson acknowledge support from an IGERT fellowship from National Science Foundation Grant DGE-0549503.

## REFERENCES

1. Y. Gotoh, M. Onoda, J. Akimoto, M. Goto, and Y. Oosawa, *Prog. Solid State Chem.* 31, 3946 (1996).
2. A. Lafond, C. Deudon, A. Meerschaut, and A. Sulpice, *Eur. J. Solid State Inorg. Chem.* 31, 967 (1994).
3. G.A. Wiegers, *Prog. Solid State Chem.* 24, 1 (1996).
4. J. Rouxel, Y. Moeelo, A. Lafond, F.J. DiSalvo, A. Meerschaut, and R. Roesky, *Inorg. Chem.* 33, 3358 (1994).
5. J.-L. Pouchou, *Microchim. Acta* 138, 133 (2002).
6. T. Phung, *X-ray Spectrom.* 37, 608 (2008).
7. L.J. van der Pauw, *Philips Res. Rep.* 13, 1 (1958).
8. L.J. van der Pauw, *Philips Tech. Rev.* 20, 220 (1958).
9. S.D. Walck and J.P. McCaffrey, *Thin Solid Films* 308, 399 (1997).
10. O. Yamashita and N. Sadatomi, *Jpn. J. Appl. Phys.* 38, 6394 (1999).